Available online at www.sciencedirect.com
ScienceDirect
Journal of Power Sources 160 (2006) 1320–1328
JOURNAL OF POWER SOURCES
www.elsevier.com/locate/jpowsour

A novel composite microporous polymer electrolyte prepared with molecule sieves for Li-ion batteries

Yan-Xia Jiang [a,*], Zuo-Feng Chen [a], Quan-Chao Zhuang [a], Jin-Mei Xu [a], Quan-Feng Dong [a,b], Ling Huang [a], Shi-Gang Sun [a,*]

[a] *State Key Laboratory of Physical Chemistry of Solid Surfaces, Department of Chemistry, College of Chemistry and Chemical Engineering, Xiamen University, #422, South Road of Siming, Xiamen 361005, China*
[b] *Powerlong Battery Research Institute, Xiamen University, Xiamen 361005, China*

Received 14 September 2005; received in revised form 7 February 2006; accepted 10 February 2006
Available online 19 May 2006

Abstract

Molecular sieves of NaY, MCM-41, and SBA-15 were used as fillers in a poly(vinylidene fluoride-*co*-hexafluoropropylene) (PVdF-HFP) copolymer matrix to prepare microporous composite polymer electrolyte. The SBA-15-based composite polymer film was found to show rich pores that account for an ionic conductivity of 0.50 mS cm^{-1}. However, the MCM-41 and NaY composite polymer films exhibited compact structure without any pores, and the addition of MCM-41 even resulted in aggregation of fillers in the polymer matrix. These differences were investigated and interpreted by their different compatibility with DMF solvent and PVdF-HFP matrix. Results of linear sweep voltammetry (LSV), electrochemical impedance spectroscopy (EIS), X-ray diffraction (XRD) and differential scanning calorimetry (DSC) have revealed that the addition of SBA-15 has extended the electrochemical stability window of polymer electrolyte, enhanced the interfacial stability of polymer electrolyte with lithium electrode, and inhibited also the crystallization of PVdF-HFP matrix. Half-cell of Li/SBA-15-based polymer electrolyte/MCF was assembled and tested. The results have demonstrated that the coulombic efficiency of the first cycle was around 87.0% and the cell remains 94.0% of the initial capacity after 20 cycles, which showed the potential application of the composite polymer electrolyte in lithium ion batteries.

Keywords: Composite microporous polymer electrolyte; Mesoporous sieves; PVdF-HFP; Lithium ion batteries; Interfacial properties

1. Introduction

Polymer lithium ion batteries (PLIB), commonly referred to the second generation lithium ion batteries, have received extensive attention since their first introduction by Bellcore Corp. [1,2]. The concept suggested by Bellcore Corp. to construct a PLIB is based on the preparation of a microporous polymer, and the immobilization of liquid electrolyte in the microporous polymer matrix. Nowadays, the separators in the Bellcore's system are prepared with extraction step, i.e., the poly(vinylidene fluoride-*co*-hexafluoropropylene) (PVdF-HFP)/plasticizer (such as dibutyl phthalate (DBP)) gel-blend film was prepared firstly, then the plasticizer was removed by liquid extraction using a low boiling point solvent, leaving the porous matrix in the film. The extraction step will nevertheless complicate the industrial production process, and it is not easy to remove all the residual plasticizer in a drying step due to the high boiling point of the plasticizer. As a result, a poor cyclability performance of the cell is encountered. Phase inversion [3,4] is another method commonly used to prepare the microporous film. In this method, double solvents with different volatility and dissolvability for PVdF-HFP are used to form phase separation in the drying course of the mixed solution. In comparison with the Bellcore's technique, phase inversion can avoid a complex extraction step, yet this method requests strict conditions of temperature and humidity to control the solvents evaporation. It tends to fail in a minor poorly controlled condition. As a consequence, the technique of phase inversion has not been applied in industrial processes. In order to improve the technique further, substantial research efforts have been addressed [5,6], and different methods were introduced in preparing the PVdF-HFP

* Corresponding authors. Tel.: +86 592 2180181; fax: +86 592 2183047.
E-mail addresses: yxjiang@xmu.edu.cn (Y.-X. Jiang), sgsun@xmu.edu.cn (S.-G. Sun).

0378-7753/$ – see front matter © 2006 Published by Elsevier B.V.
doi:10.1016/j.jpowsour.2006.02.029

microporous film. As an example, Prosini et al. [5] developed a new class of microporous film, where γ-$LiAlO_2$, Al_2O_3 and MgO were used as fillers in a PVdF-HFP polymer matrix to form self-standing, intrinsically porous separators for lithium ion batteries.

Silica, such as SBA-15 [7] and MCM-41 [8], is a new type of mesoporous molecular sieve that has been synthesized in the last decade. These materials possess a highly ordered hexagonal arrangement of cylindrical mesopores that provide the ease of entrance and transfer of ions or molecules in comparison with microporous zeolite [9]. The mesopore structure also brings on a much larger surface area than that of common materials. In addition, the framework unit of SBA-15 or MCM-41 consists of SiO_2, and possesses steady electrochemical properties. In comparison with MCM-41, SBA-15 exhibits even large pore diameter and thick pore walls that result in a more stable structure. Moreover, since SBA-15 is synthesized by using triblock copolymers' template, removal of the polymer would lead to the development of irregular intrawall pores, i.e., SBA-15 generally possesses rough pore walls with micro- and narrow mesopores that coexist with the regular hexagonal framework of main channels, as has been shown by Kruk and co-workers [10] and Ravikovitch and Neimark [11]. These characteristics make SBA-15 exceedingly useful. Thanks to their numerous merits, these mesoporous materials have been applied with considerable attention in rechargeable lithium or lithium ion batteries. Reddy and Chu et al. [12,13] explored the modification of a polyethylene oxide (PEO) with mesoporous SBA-15 or MCM-41, and studied the conduction mechanism of ions in the composite system. It has been confirmed that the incorporation of MCM-41 or SBA-15 in a PEO–$LiClO_4$ polymer electrolyte will facilitate salt dissociation, enhance ionic conductivity, and improve miscibility between organic and inorganic moieties. In addition, ^{7}Li NMR study revealed that parts of lithium ions were transferred via the surface (both interior and exterior) of the mesochannels.

In the current paper, we developed a new technique without extraction step and without special requirements for temperature and humidity in preparation of a composite microporous polymer electrolyte involving different kinds of molecule sieves. The characterization results concerning the micropores formation mechanism, the electrochemical behavior including ionic conductivity, electrochemical stability window, interfacial property, cyclability performance, as well as the compatibility between PVdF-HFP matrix and different molecule sieves were described.

2. Experimental

2.1. Materials

A copolymer of PVdF-HFP, trade mark Kynar 2801, was purchased from Elf Atochem. Mesoporous SBA-15 (150(d) nm × 400(h) nm particle size), MCM-41 (100(d) nm × 300(h) nm particle size) and microporous NaY (500 nm particle size) were used as filler to prepare composite films. The PVdF-HFP was further purified by heating under vacuum at 70 °C and the molecule sieves were dried at 200 °C for 12 h before use. An electrolyte solution with 1 M $LiPF_6$ in EC/DMC/EMC (volume ratio 1:1:1) was supplied by Mitsubishi Chemical. All other chemicals are of analytical grade.

2.2. Membrane preparation

A certain amount of molecule sieve powder was dispersed in DMF solvent by ultrasonic, and then the PVdF-HFP powder of 0.40 g was dissolved in the above mixture by stirring. After complete dissolution, the mixture was cast on a smooth cleaned glass plate with the approach of self-spread. The solvent was evaporated in a dry atmosphere and followed by drying under vacuum to form a film (about 80 μm in thickness), designated as "dry film". The dry film thus obtained was activated in a glove box (MIKROUNA, $H_2O < 1$ ppm, $O_2 < 4$ ppm) by adding liquid electrolyte, designated as "wet film". For comparison purpose, microporous film by extraction step (i.e., by the Bellcore's technique), where DBP and methanol were selected as plasticizer and extractor, respectively, was also prepared. In comparison with the Bellcore's technique, the approach of preparation of microporous membranes in this work is denominated as the direct-making-pore technique (DMPT).

2.3. Characterization and instruments

Porosity of the as-prepared membrane was measured by following procedure: (1) immerse the dry film into n-butanol for 2 h, (2) weigh the mass of membrane before and after absorption of n-butanol, and (3) calculate the porosity of membrane by using the equation $P\% = (W_w - W_d)/(\rho_b V_p)$, where W_w and W_d are, respectively, the mass of the wet and dry films, ρ_b the density of n-butanol, and V_p is the volume of the dry film. The electrolyte uptake, R_A, was defined as the ratio of the mass of absorbed electrolyte solution (m_s) to the mass of the dry film (m_p), i.e., $R_A = m_s/m_p$. The ionic conductivity of the composite film was determined by electrochemical impedance spectroscopy, in which the wet film was sealed between two stainless steel (SS) electrodes and the measurements were carried out in the frequency range form 100 KHz to 10 Hz. The bulk resistance of the polymer electrolyte was evaluated from impedance spectra. The ionic conductivity was calculated by using the equation: $\sigma = L/(RS)$, where σ is the ionic conductivity, R the bulk resistance, L and S are the thickness and the area of the specimen, respectively. Measurements of temperature dependence were conducted in the range from 20 °C to 80 °C. Before each point of test, the system was kept at the corresponding temperature for about 30 min to reach the thermal balance. To evaluate the anodic stability of the composite film, a cell was prepared by sandwiching manner, namely the wet film is being in the middle of a SS electrode and a lithium foil. The electrochemical stability was tested by slowly increasing the cell voltage until the onset of current appearance. The voltage was swept from open circuit voltage (OCV) towards a more anodic potential with a scan rate of 1 mV s^{-1}. The interfacial stability of lithium electrode/polymer electrolyte was evaluated by monitoring the impedance response of the assembly cells. These cells were stored under open circuit conditions and the

impedances were measured over a 100 Hz to 10 KHz frequency range with amplitude of voltage perturbation of 5 mV. All above electrochemical experiments were performed on a CHI660B electrochemical workstation (Chenhua Corp., Shanghai, China) unless stated otherwise.

Surface morphologies of the composite films were observed by using scanning electron microscope (SEM, LEO 1530) with gold sputtered-coated films. Cross-sectional views of the membranes were obtained by breaking them in liquid nitrogen. Fourier transform infrared (FTIR) transmission spectroscopic measurements were carried out on a Nexus 870 FTIR spectrometer (Nicolet Corp.) equipped with an EverGlo^{TM} IR source and a liquid nitrogen-cooled MCT-A detector. A home-made IR transmission cell was employed with two CaF_2 disks used as the IR windows, and the samples were sealed between the two CaF_2 disks in a sandwiched manner. The resulting spectrum was expressed as absorbance, i.e., $A = -\log(R_{Si}/R_B)$, where R_{Si} is the transmission single-beam spectrum of sample, and R_B is the single-beam spectrum of background. X-ray diffraction (XRD) patterns, recorded in both small and wide angle, were obtained on an X' pert PRO (Japan) diffractometer. Thermal properties of the composite polymer membranes were studied by using a differential scanning calorimeter (NETZSCH STA 409 PC/PG, Netzsch Corp., Germany). The samples for the DSC test were placed in non-hermetric aluminum pans and then scanned from 20 °C to 190 °C at a heating rate of 10 °C min^{-1}. The melting enthalpy (ΔH_m) of samples was obtained by integrating the endothermic peak in DSC curves.

The charge and discharge tests were carried out on electrochemical workstation (Xinwei Corp., Shenzhen, China) at a constant current density and within the voltage range of 1.5–0.002 V. The anode used was lithium metal. The cathode active material was mesophase-pitch-based carbon filer (MCF) with carbon black and PVdF-HFP used as conductivity aid and binder, respectively. The cathode slurry involving the above material was obtained by *N*-methylpyrrolidone (NMP) as solvent in a special ratio and then cast on a treated copper current collector, followed by drying under vacuum and punching. The SBA-15-based film (SBA-15: PVdF-HFP = 3:8 in weight ratio) was activated and used as separator and electrolyte between the cathode and the anode to form a coin cell, that is denoted as Li/SBA-15-based separator/MCF.

3. Results and discussion

3.1. Morphologies of the composite films

SEM images of the composite films are shown in Fig. 1. The surface and cross-section of the SBA-15 composite film are displayed in Fig. 1(a and b), respectively. It can be seen that the SBA-15 composite film exhibits uniform network-like micropores structure. The average size of the pore diameter of the sample is measured as less than 10 μm. On the contrary, the addition of MCM-41 resulted in aggregation of the filler and produced scarcely micropores structure in the polymer electrolyte system, seen from Fig. 1(c). The NaY composite

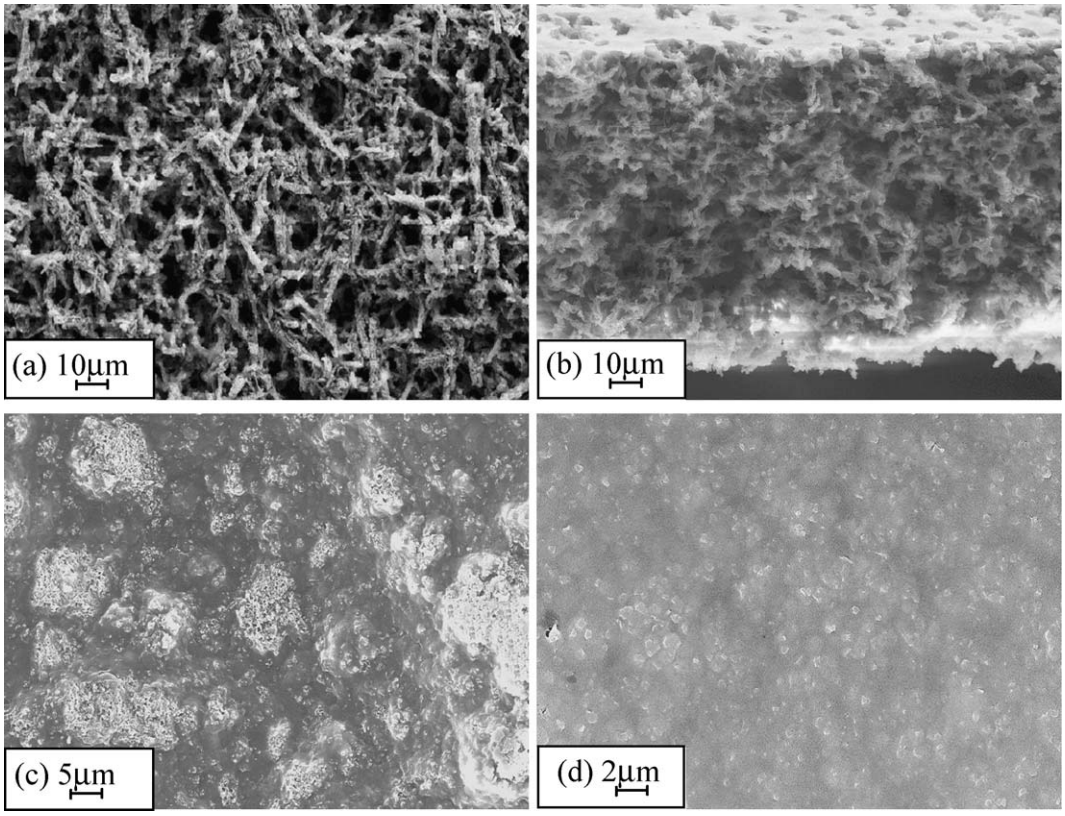

Fig. 1. SEM images of composite polymer membranes with different molecule sieves: (a) 0.15 g SBA-15; (b) and its cross-section; (c) 0.15 g MCM-41; (d) 0.15 g NaY.

Table 1
Comparison of porosity, electrolyte uptake, and ionic conductivity of composite polymer electrolytes containing different molecular sieves

	SBA-15					MCM-41	NaY
	0.20 g	0.15 g	0.10 g	0.05 g	0.00 g	0.15 g	0.15 g
Porosity (%)	59.4	45.8	24.8	12.5	3.3	14.2	8.7
Electrolyte uptake (%)	76.0	50.2	28.5	17.7	11.8	30.8	38.5
Conductivity (mS cm^{-1})	0.83	0.50	0.055	0.004	0.001	0.046	0.003

polymer membrane also displays compact structure, but without aggregation phenomenon (Fig. 1(d)). It is obvious that different molecule sieves have remarkable different impacts on the morphology of membranes, which may be ascribed to their respective structure, as well as their different compatibility with solvent DMF and PVdF-HFP.

3.2. Porosity, electrolyte uptake, and ionic conductivity

The porosity, electrolyte uptake, and ionic conductivity of the composite films are characterized by experimental data listed in Table 1. SBA-15 composite film was investigated particularly by adding different masses of the filler. It can be found that the parameter values were all increased rapidly with the increase of SBA-15 mass. In the case of the composite film containing 0.15 g SBA-15, the ionic conductivity reached 0.5 mS cm^{-1} at room temperature, which is about 2–3 orders of magnitude larger than that of the blank film without any fillers. It is worthwhile to note that a skin layer was formed at one side of the film that contacted with the glass substrate. Such skin layer will inhibit the increase of ionic conductivity of the film. It can be seen that with further increase of the mass of SBA-15 to 0.20 g, though the ionic conductivity kept improving, the mechanical strength was deteriorated to a certain extent. To get a favorable membrane of high porosity and strong mechanical strength, the addition of 0.15 g SBA-15 was found to be suitable. For comparison, the parameters of the composite films with the same mass of 0.15 g MCM-41 and NaY were also measured and listed in Table 1.

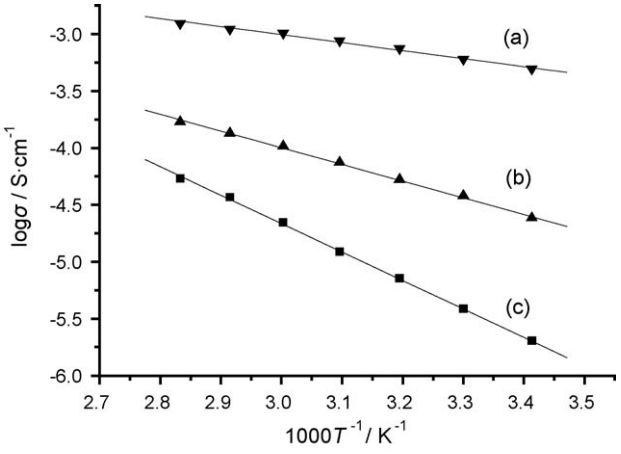

Fig. 2. Arrhenius plots of ionic conductivity for the composite films of: (a) 0.15 g SBA-15; (b) 0.15 g MCM-41; (c) 0.15 g NaY. Experimental data are shown as symbols and theoretical data obtained from curve linear fitting are shown as solid lines.

The ionic conductivity of MCM-41 composite film was measured about one order of magnitude larger than that of the NaY composite film. From SEM images and porosity values of the two composite films, it may be suggested that the relatively large ionic conductivity of the MCM-41 composite film is associated with interspaces formed by the aggregation of MCM-41 fillers, where the ions are mainly conducted.

The temperature dependence of the ionic conductivity, i.e., the plot of $\log\sigma$ versus T^{-1}, is illustrated in Fig. 2. It can be observed that the three plots are all approximately linear, suggesting the Arrhenius-like behavior of ionic conduction within a limited temperature range (20–80 °C). However, diversity of the plot slopes, which represent the magnitude of the activation energy (E_a), can be differentiated among them. The SBA-15 composite film holds obviously the lowest E_a, suggesting the fastest mobility of conducting ions in it.

3.3. FTIR studies of the formation mechanism of micropores

In order to figure out the formation mechanism of micropores in the films, FTIR transmission spectroscopic studies were carried out. Fig. 3(a) displays the IR spectrum of DMF solvent, the absorption bands appearing around 1657–1696 cm^{-1} were ascribed to IR absorption of C=O double bonds [14]. Fig. 3(b

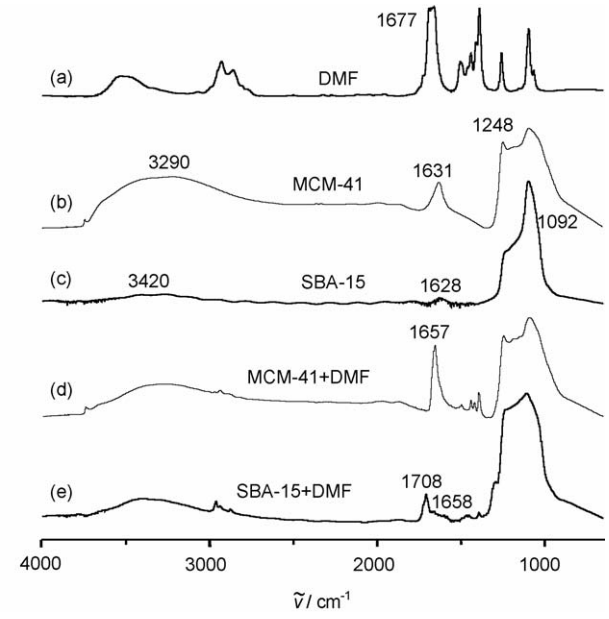

Fig. 3. The IR spectra of: (a) DMF; (b) MCM-41; (c) SBA-15; (d) MCM-41 containing a little DMF; (e) SBA-15 containing a little DMF.

and c) shows IR absorption spectra of the mesoporous sieves of MCM-41 and SBA-15, respectively. Two IR absorption bands near 3290 cm^{-1} and 1631 cm^{-1} in Fig. 3(b) may be assigned to the presence of the oxygen–hydrogen single bond (O–H), and a band near 1248 cm^{-1} can be assigned to the silicon–oxygen single bond (Si–O) [15]. Similarly, the corresponding bands can be also observed at 3420 cm^{-1}, 1628 cm^{-1}, and 1092 cm^{-1} [16] in the spectrum of SBA-15 (Fig. 3(c)). Though similar IR characters are present in both spectra of pure MCM-41 and SBA-15, the IR spectral features are quite different when a small quantity DMF solvent was added as shown, respectively, in Fig. 3(d and e). In the case of MCM-41 containing DMF, the original IR features belonging to O–H group in MCM-41 and C=O group in DMF were merged into one band around 1657 cm^{-1}, which is located in the middle between the two original bands. It is reasonable to consider that such a combination of bands is a simple physical overlapping, instead of bands displacement. This result suggests that there is no interaction between MCM-41 and DMF. However, the presence of DMF in SBA-15 makes the O–H IR band of 1628 cm^{-1} shifting positively to 1658 cm^{-1} and becoming broad. In addition, a positive-shift of 31 cm^{-1} is also measured for the C=O band. These variations may be associated to the interaction between Si–OH in SBA-15 and nitrogen atom in DMF solvent. Such interaction will induce the adsorption of DMF inside and outside the SBA-15 mesochannel, then bring on the SBA-15 into solvate, and finally engender a new type of solvent phase around SBA-15.

Based on the above results and discussion, it can be presumed that there may exist two states of solvent in the mixture of DMF, PVdF-HFP, and SBA-15, i.e., simple solvent state of DMF (DMF_{sol}) and the solvent state of DMF adsorbed around SBA-15 ($DMF_{SBA\text{-}15}$). The former possesses a low boiling point and exhibits a strong solvency for PVdF-HFP, whereas the latter is in the reversed situation. In comparison with the phase inversion in a common sense, the formation mechanism of micropores in the SBA-15 composite film can be suggested as following. Since the boiling point of $DMF_{SBA\text{-}15}$ is much higher than that of DMF_{sol}, the mass of $DMF_{SBA\text{-}15}$ and PVdF-HFP may keep invariable while the DMF_{sol} is vaporizing when the confected mixture is cast on a newly cleaned glass plate. With the evaporation of DMF_{sol}, the system of the confected mixture comes into the mesophase region, and initiates further a disassembling phenomenon, sequentially forming the rich and deficient phases of the PVdF-HFP. The polymer in the rich phase gradually crystallizes to form the polymer matrix; simultaneously the deficient phase turns into micropores infilling in the polymer film. At the end of the phase inversion, PVdF-HFP and SBA-15 in the deficient phase attach to the matrix, producing the SBA-15 fillers covered with PVdF-HFP.

3.4. XRD characterization of composite films

Microporous NaY exhibits a very stable structure, and it can maintain the stability in the whole process of composite film preparation. For the mesoporous silica, it is necessary to test their stability in the composite system. Fig. 4 displays the small angle XRD patterns of the composite films of mesosiliceous

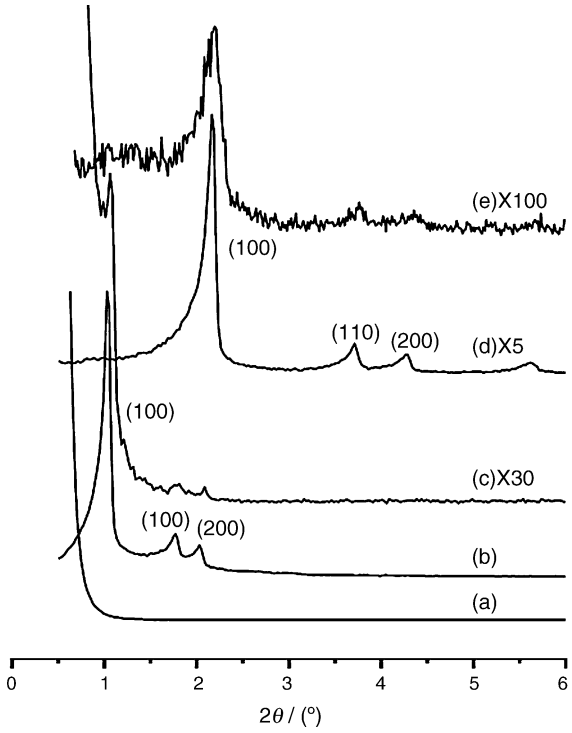

Fig. 4. Small angle XRD patterns of: (a) PVdF-HFP blank film; (b) SBA-15 powder; (c) SBA-15 composite film; (d) MCM-41 powder; (e) MCM-41 composite film.

materials. The XRD pattern of the PVdF-HFP blank film shown in Fig. 4(a) does not exhibit obviously any diffraction peaks, account for non-interfering analysis for the mesoporous silica in the small angle. The SBA-15 powder exhibits the structure of typical hexangular phase at 2θ in the range of 0.5–2° (see Fig. 4(b)), attributed to the characteristic diffraction peaks of (1 0 0), (1 1 0), and (2 0 0), respectively [7]. We can still observe the characteristics of these three crystal planes in SBA-15 composite film by enlargement (see Fig. 4(c)), which indicates that the ordered mesochannel arrangement of SBA-15 has not been destroyed during the composite film preparation. The reduction in intensity may be due to the existence of PVdF-HFP inside and outside the SBA-15 channel. The same phenomena can be observed in the MCM-41 powder and its composite film shown in Fig. 4(d and e), indicating that the ordered structure of MCM-41 is still maintained though MCM-41 is much more vulnerable than SBA-15. Similar results concerning the stability of the structure of mesoporous silica were reported also in solid polymer electrolyte [13], where the long-range order between the SiO_2 channels in mesoporous silica are preserved in large surplus of the PEO/$LiClO_4$ electrolyte. In the present work, the maintenance of the special ordered mesostructure of SBA-15 takes on basilic significance for the formation of micropores in the composite film.

Fig. 5 displays XRD patterns of wide angle of different materials including PVdF-HFP powder, PVdF-HFP blank film, SBA-15 composite film, MCM-41 composite film, and NaY composite film. These XRD patterns depict the change in crystallinity of samples. The characteristic diffraction peaks of semi-crystalline PVdF-HFP powder appear between $2\theta = 15°$ and 40°, and com-

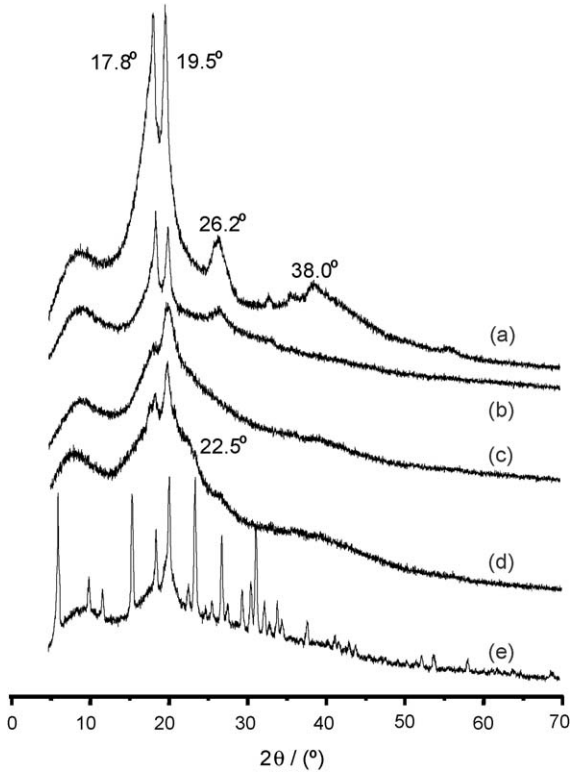

Fig. 5. Wide angle XRD patterns of: (a) PVdF-HFP powder; (b) PVdF-HFP blank film; (c) SBA-15 composite film; (d) MCM-41 composite film; (e) NaY composite film.

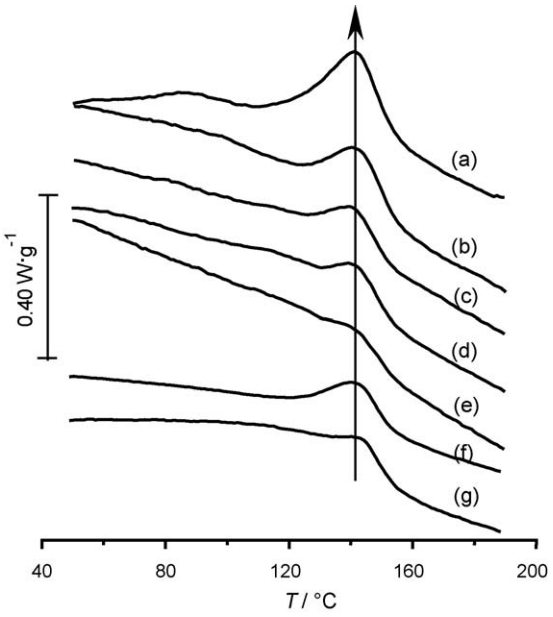

Fig. 6. The DSC curves of: (a) PVdF-HFP powder; and the composite films with different molecule sieves; (b) 0.00 g SBA-15; (c) 0.05 g SBA-15; (d) 0.10 g SBA-15; (e) 0.15 g SBA-15; (f) 0.15 g MCM-41; (g) 0.15 g NaY. The arrow indicates the endothermic direction.

prise two sharp diffraction peaks at $2\theta = 17.8^\circ$ and 19.5°, as well as two broad diffraction peaks at $2\theta = 26.2^\circ$ and 38° (Fig. 5(a)), which were associated with the (1 0 0) + (0 2 0), (1 1 0), (0 2 1) and (0 0 2) reflections of crystalline PVdF, respectively [17–19]. These diffraction peaks become less prominent and the diffraction peak at $2\theta = 38.0^\circ$ disappears in the PVdF-HFP blank film (Fig. 5(b)), indicating the decrease in crystallinity degree during the transformation of the polymer conformation. With the addition of SBA-15 to PVdF-HFP polymer, the intensity of diffraction peaks decreases further together with the disappearance of the diffraction peak at $2\theta = 26.2^\circ$ and the transformation of the diffraction peak at $2\theta = 17.8^\circ$ into one hump (Fig. 5(c)). The results indicate that the crystallinity degree of PVdF-HFP is further reduced by the addition of mesoporous SBA-15. In the case of MCM-41 composite film, a prominent diffraction peak at $2\theta = 17.8^\circ$ can be observed in Fig. 5(d), which implies comparatively a higher crystallinity degree in the MCM-41 composite film than that of the SBA-15 composite film. In addition, a featureless broad bump appears in the same XRD pattern around $2\theta = 22.5^\circ$, which is ascribed to the amorphous phase of SiO_2. Since this amorphous phase of SiO_2 was not visible in the XRD pattern of SBA-15 composite film, it is reasonable to suggest that the exposure of the aggregated MCM-41 in the film induced the visualization of the peak corresponding to SiO_2 amorphous phase. Fig. 5(e) shows the XRD pattern of NaY composite film, in which the strong diffraction peaks are ascribed to characteristic diffraction peaks of NaY and the undulate baseline attributes to the characteristic diffraction peaks of semi-crystalline PVdF-HFP. The undulate baseline affirms the significant reduction of crystallinity degree of PVdF-HFP in the NaY composite film. The depression of the crystallization, which is also one of goals of adding different fillers, is very important for polymer electrolyte, since it will lead to the increase of amorphous phase of polymer electrolyte. As a consequence, a high affinity to electrolyte solution and an enhanced ionic conductivity were obtained. In this sense, SBA-15 and NaY are better ceramic fillers than MCM-41.

3.5. Studies of thermal properties

In order to further investigate quantitatively the evolvement of crystallinity of the composite films, DSC of these samples was measured. Fig. 6 shows the DSC thermograms of PVdF-HFP powder and its composite films. The results of DSC analysis are summarized in Table 2. In fact, it is difficult to determine the T_g (the glass transition temperature) of PVdF-HFP because it is semi-crystalline. However, the position and intensity change of the melting peak of samples can be observed. The PVdF-HFP powder shows an endothermic peak at 141.1 °C, which is attributed to its melting. When the powder was made into membrane, the melting enthalpy undergone a sharp decrease and the endothermic peak was slightly shifted negatively by 1 °C. By further variation of addition of different masses of SBA-15, the composite films display broader endothermic peaks at a low temperature from 140.1 °C to 139.4 °C and a low melting enthalpy from 16 J g^{-1} to 7.32 J g^{-1}, which reflects a decrease in crystallinity degree. The negative-shift of the melting peak and the reduction of the fusion heat indicate that the SBA-15 is compatible with PVdF-HFP to a certain extent. Moreover, the addition of 0.15 g NaY can also induce the decrease in the

Table 2
The melting peak position and melting enthalpy of PVdF-HFP powder and its composite films

	PVdF-HFP powder	PVdF-HFP composite films					
		SBA-15				MCM-41	NaY
		0.00 g	0.05 g	0.10 g	0.15 g	0.15 g	0.15 g
Melting peak position, T (°C)	141.1	140.1	139.8	139.5	139.4	139.5	139.5
Melting enthalpy, ΔH_m (J g^{-1})	23.21	16	13.34	10.62	7.32	12	9.2

degree of crystallinity of PVdF-HFP with a relatively low value of 9.2 J g^{-1}, whereas MCM-41 gets a high value of 12 J g^{-1}, illustrating their different compatibility with PVdF-HFP.

The above DSC results were generally in accordance with the XRD results, and they can be also interpreted from the SEM images. SBA-15 and NaY composite films both exhibit uniform surface morphology, implying their good compatibility with polymer matrix, no matter whether the pores were present. Contrarily, MCM-41 composite film exhibits rough surface morphology with grievous aggregation, reflecting its bad compatibility with polymer matrix. The different compatibility can be further associated with respective structure of the sieve fillers, as well as those results in the above IR analysis. In comparison with MCM-41, the SBA-15 possesses larger pores and larger surface area. It may be easy for DMF solvent absorbing on the surface of SBA-15, which is beneficial to make SBA-15 into solvate. SBA-15 owns also rough pore walls with micro- and narrow mesopores that coexist with the main channels of the regular hexagonal structure of cylinder, such structure will also account for a strong affinity between SBA-15 and DMF solvent. The close coalescent between SBA-15 and DMF can prevent the fillers into conglomeration, benefit the approach of PVdF-HFP towards SBA-15, and finally reach a favorable compatibility between SBA-15 and PVdF-HFP. As far as the NaY, it has much higher particle density than that of mesoporous silica, and the NaY composite polymer solution obviously manifests higher viscousness than those of SBA-15 and MCM-41, so it is difficult for these heavier particles to move into conglomeration, i.e., the NaY particles can also disperse uniformly in polymer film. The well dispersion of the particles will block the continuous crystallinity growth of polymer, thus the good compatibility between them can be obtained.

3.6. The electrochemical stability window of SBA-15 composite film

It is obvious that the SBA-15 composite film exhibits the highest ionic conductivity and the best compatibility between polymer matrix and fillers among the three composite films studied. It is of importance also to obtain a wide and stable electrochemical window and a favorable interfacial behavior between SBA-15 composite film and electrode to ensure the acceptable performance for rechargeable batteries of high energy density [20].

Linear sweep voltammograms recorded with a cell of lithium/polymer electrolytes/SS are used to evaluate the electrochemical stability of polymer electrolytes, and are presented in Fig. 7. A very low background current about 3 μA was measured in potential region between 2 V and 4.2 V, it was increased to approximately 5 μA at 4.5 V for the SBA-15 composite film (Fig. 7(b)) made by DMPT. Upon further increase of the cell voltage to 5.0 V, a considerable current began to flow, indicating the onset of electrolyte decomposition process. Whereas, the decomposition voltage of the polymer electrolyte made by extraction step without any fillers (see Fig. 7(a)) is found to be 4.8 V with a small notched current at low voltage, which is attributed to the oxidation of some impurity trace, such as water and oxygen. The facts of the non-notched background current and the higher decomposition voltage in SBA-15 composite polymer electrolyte indicate that, on the one hand, the SBA-15 powders have no deficient effect on electrochemical stability window of the electrolyte, and on the other hand, the SBA-15 powders may absorb trace impurity in the electrolyte, leading to a cleaner system and a higher decomposition voltage.

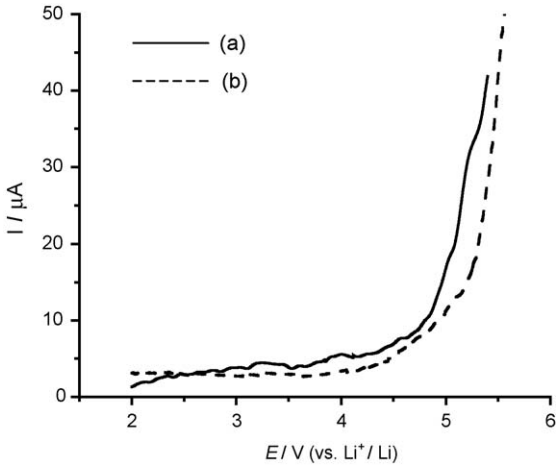

Fig. 7. Linear sweep curves of polymer electrolytes, scan rate—1 mV s^{-1}: (a) microporous film made by extraction step without any fillers and (b) 0.15 g SBA-15 composite film made by DMPT.

3.7. Interfacial property with lithium electrode

It is very important for the safety and cyclability performance of batteries to obtain an improved interfacial property between lithium electrode and the polymer electrolyte. Impedance spectroscopy is a convenient tool for monitoring interfacial phenomena. The time evolution of the impedance response was monitored with Li/electrolyte/Li cells at open circuit for 12 days. Fig. 8 shows the progressive expansion of the depressed semicircles with time. The depressed semicircles are associated

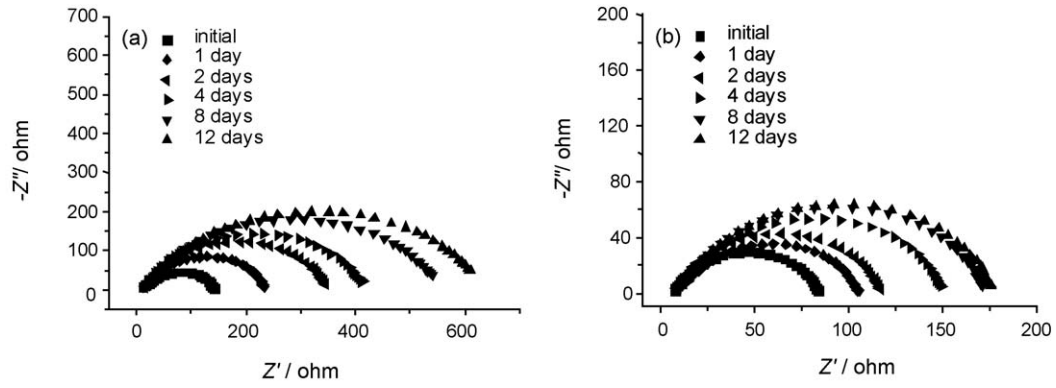

Fig. 8. Impedance response of a Li/CMPE/Li cell at progressive storage time: (a) microporous film made by extraction step without any fillers and (b) 0.15 g SBA-15 composite film made by DMPT. The semicircles from internal to external are, respectively, initial, 1 day, 2 days, 4 days, 8 days, and 12 days.

with the passivation layer and the charge transfer resistances on the lithium electrode, which are considered to constitute the interfacial resistance (R_{int}) [21]. The difference is quite considerable between Fig. 8(a and b), since only small changes in the amplitude of the relevant semicircle are observed over prolonged storage time in the cell using the SBA-15 composite electrolyte prepared in this work comparing with that of the cell employing an electrolyte made by extraction step. It is obvious that the addition of the SBA-15 fillers reduced the rate of growth of the resistive layer on the Li surface. This beneficial interfacial characteristic has further affirmed that the addition of the SBA-15 fillers can trap residual trace of impurities such as water and oxygen, and prevent them from reacting at the interface. It may be worth reporting that this 'interfacial stabilizing' effect of the ceramic fillers has been also identified in other laboratories [22–24].

3.8. Cyclability of lithium ion batteries

In order to verify the electrochemical performance of the composite polymer electrolytes, coin cells of Li/SBA-15-based separator/MCF were assembled to test their performance of charge–discharge cycling. The charge–discharge curve of the first preconditioning cycle at the 0.1 C rate and further cycles of the 2nd, 10th and 20th at the 0.5 C rate between 1.5 V and 0.002 V are shown in Fig. 9. It can be seen that the charge–discharge plateau is stable. The coulombic efficiency (defined as the ratio of the charge capacity to discharge capacity) of the first cycle was around 87.0% that is attributed to the formation of SEI film, whereas the value reached as high as 98% for the 20th cycle. It should be pointed out that the capacity fall of charge between the first cycle and the second cycle was associated with the current rate. The large current rate easily results in polarization that reduces the charge capacity. The relative values of charge capacities as a function of cycle numbers from 2 to 20 are shown in Fig. 10. The charge capacity decreased slightly and remained 94.0% of the initial capacity of the 2nd cycle after 20 cycles, demonstrating a good cyclability performance of Li/SBA-15-based separator/MCF cell.

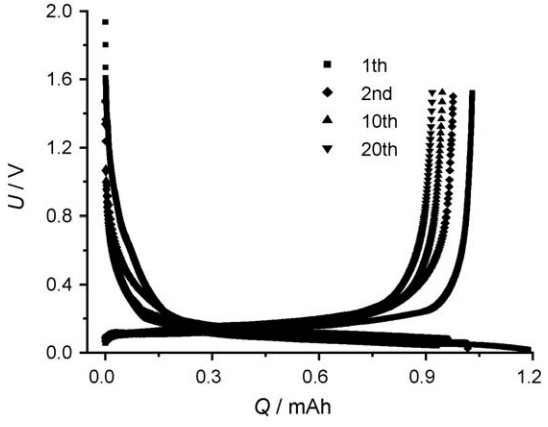

Fig. 9. Charge–discharge curves of the Li/SBA-15-based separator/MCF cell of the 1st cycle at the 0.1 °C rate, and the 2nd, 10th, and 20th cycle at the 0.5 C rate.

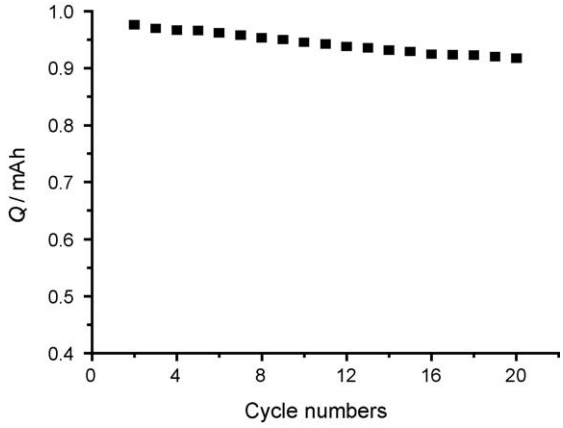

Fig. 10. Long-term cycling tests of the Li/SBA-15-based separator/MCF cell at the 0.5 C rate.

4. Conclusion

Composite microporous polymer electrolytes based on different molecule sieves (SBA-15, MCM-41, and NaY) and PVdF-HFP were prepared. SBA-15-based composite polymer electrolyte was found to be intrinsically porous and provided an ionic conductivity of 0.50 mS cm^{-1} at room temperature. Studies of

infrared transmission spectroscopy suggested the mechanism of micropores formation, i.e., the interaction between Si–OH in SBA-15 and nitrogen atom in DMF solvent led to the formation of micropores. Such interaction was not nevertheless observed on MCM-41 system. The fillers of SBA-15, MCM-41 and NaY show different compatibility with PVdF-HFP: SBA-15 and NaY can disperse uniformly in the composite films and inhibit the crystallization of PVdF-HFP to a large extent, while the MCM-41 aggregates together and cannot reduce effectively the crystallinity degree. The results have revealed also that the addition of the SBA-15 does not change the electrochemical stability window; on the contrary, it can absorb trace impurity in the electrolyte, and affect efficiently the growth of the passivation layer on the lithium electrode. The battery of Li/SBA-15-based separator/MCF was assembled to test the performance of the composite film. The coulombic efficiency of the first cycle was measured around 87.0% and the cell remains 94.0% of the initial capacity after 20 cycles, which demonstrated the potential application of the composite polymer electrolyte in lithium ion batteries.

Acknowledgements

The studies were supported by the National Key Basic Research and Development Program (Grant No. 2002CB-211804), the National Natural Science Foundation of China (Grants Nos. 90206039, 20433040, and 20573085).

References

[1] A.S. Gozdz, C.N. Scumutz, J.M. Tarascon, US Patent 5,296,318 (1993-03-06).
[2] J.M. Tarascon, A.S. Goztz, C. Schmutz, F. Shokoohi, P.C. Warren, Solid State Ionics 86–88 (1996) 49–54.
[3] V. Arcella, A. Sanguineti, E. Quartarone, P. Mustarelli, J. Power Sources 81–82 (1999) 790–794.
[4] Q. Shi, M.X. Yu, X. Zhou, Y.X. Yan, C.R. Wan, J. Power Sources 103 (2002) 286–292.
[5] P.P. Prosini, P. Villano, M. Carewska, Electrochim. Acta 48 (2002) 227–233.
[6] D.W. Kim, Y.K. Sun, J. Power Sources 102 (2001) 41–45.
[7] D.Y. Zhao, J.L. Feng, Q.H. Huo, N. Melosh, G.H. Fredrickson, B.F. Chmelka, G.D. Stucky, Science 279 (23) (1998) 548–552.
[8] C.T. Kresge, M.E. Lonowicz, W.J. Roth, J.C. Vartuli, J.S. Beck, Nature 359 (1992) 710–712.
[9] J. Weitkamp, Solid State Ionics 131 (2000) 175.
[10] M. Kruk, M. Jaroniec, C.H. Ko, R. Ryoo, Chem. Mater. 12 (2000) 1961–1968.
[11] P.I. Ravikovitch, A.V. Neimark, J. Phys. Chem. B 105 (2001) 6817–6823.
[12] M.J. Reddy, P.P. Chu, J. Power Sources 135 (2004) 1–8.
[13] P.P. Chu, M.J. Reddy, H.M. Kao, Solid State Ionics 156 (2003) 141–153.
[14] Z.X. Wang, B.Y. Huang, Z.H. Lu, S.M. Wang, R.J. Xue, L.Q. Chen, Solid State Ionics 92 (1996) 265–271.
[15] C. Guo, D. Zhang, G.X. Jin, Chin. Sci. Bull. 49 (3) (2004) 249–253.
[16] A.B. Bourlinos, A. Simopoulos, N. Boukos, D. Petridis, J. Phys. Chem. B 105 (2001) 7432–7437.
[17] D. Saikia, A. Kumar, Electrochim. Acta 49 (16) (2004) 2581–2589.
[18] S. Abbrent, J. Plestil, D. Hlavata, J. Lindgren, J. Tegenfeldt, Å. Wendsjö, Polymer 42 (2001) 1407–1416.
[19] A. Tawansi, A.H. Oraby, H.I. Abdelkader, M. Abdelaziz, J. Magn. Magn. Mater. 262 (2003) 203–211.
[20] C.H. Kim, K.H. Lee, W.S. Kim, J.K. Park, D.Y. Seung, J. Power Sources 94 (2001) 163–168.
[21] M. Nookala, B. Kumar, S. Rodrigues, J. Power Sources 111 (2002) 165–172.
[22] S. Slane, M.J. Salonmon, J. Power Sources 55 (1995) 7–10.
[23] G.B. Appetecchi, F. Croce, L. Persi, F. Ronci, B. Scrosati, Electrochim. Acta 45 (2000) 1481–1490.
[24] Q. Li, H.Y. Sun, Y. Takeda, N. Imanishi, J. Yang, O. Yamamoto, J. Power Sources 94 (2001) 201–205.